The formation of Mg-orthocarbonate through the reaction $MgCO_3$ + MgO = Mg_2CO_4 at Earth's lower mantle P–T conditions

Pavel N. Gavryushkin *[1,2], Dinara N. Sagatova[1,2], Nursultan Sagatov[1], and Konstantin D. Litasov[3]

[1] *Sobolev Institute of Geology and Mineralogy, Siberian Branch of Russian Academy of Sciences, prosp. acad. Koptyuga 3, 630090 Novosibirsk, Russia*

[2] *Novosibirsk State University, Pirogova 2, Novosibirsk 630090, Russia*

[3] *Vereshchagin Institute for High Pressure Physics RAS, 108840, Troitsk, Moscow, Russian Federation*

Abstract

Orthocarbonates of alkaline-earth metals are the newly discovered class of compounds stabilized at high pressures. Orthocarbonates of Ca and Mg are the potential carbon host phases, transferring oxidized carbon in the Earth's lower mantle up to the core-mantle boundary. Here, we demonstrate the possibility for the formation of Mg_2CO_4 in the lower mantle at pressures above 50 GPa, by *ab initio* calculations. Mg_2CO_4 is formed by the reaction $MgCO_3$ + MgO = Mg_2CO_4, proceeding only at high-temperatures. At 50 GPa the reaction starts at 2200 K. The temperature decreases with pressure and drops down to 1085 K at the pressure of the Earth's core-mantle boundary, near 140 GPa. Two stable structures, Mg_2CO_4-*Pnma* and Mg_2CO_4-$P2_1/c$, were revealed. Mg_2CO_4-*Pnma* is isostructural to Mg_2SiO_4 (forsterite) and stable below 80 GPa. Mg_2CO_4-$P2_1/c$ is isostructural to β-Ca_2SiO_4 (larnite) and stable above this pressure. Mg_2CO_4-*Pnma* has a melting temperature of 16-18 % higher than the melting temperature of $MgCO_3$ (magnesite). At 23.7 GPa and 35.5 GPa, Mg_2CO_4-*Pnma* melts at 2742 K and 2819 K, respectively. Acoustic wave velocities Vp and Vs of Mg_2CO_4-*Pnma* are very similar to that of magnesite, while orthocarbonate owns stronger universal anisotropy in comparison with carbonate and has a larger coefficient A^U.

*Electronic address: gavryushkin@igm.nsc.ru, p.gavryushkin@g.nsu.ru; Corresponding author

Introduction

During the recent decade, the crystal structure prediction technique became an integral part of high-pressure research. Numerous interesting experimental synthesis were guided by this technique, for instance, the synthesis of the high-pressure phases of alkaline carbonates Li_2CO_3, Na_2CO_3, and K_2CO_3 [1–3] and alkaline-earth carbonates $CaCO_3$, $MgCO_3$, and $CaMg(CO_3)_2$ [4–10].

Orthocarbonates are another example for experimental confirmation of theoretically predicted structures. The possibility for the synthesis of alkaline orthocarbonates, the salts of the not yet experimentally observed orthocarbonic acid, has been suggested from the theoretical considerations [11, 12]. However, these predictions are still unverified by the experiment. The stability of the alkaline-earth orthocarbonates has not been considered till the last year. The performed crystal structure prediction in the MgO – CO_2 and CaO – CO_2 systems have revealed sp^3-bonded structures with the intermediate stoichiometries, Ca_3CO_5 and CaC_2O_5, stabilized at high pressures [13]. Thermodynamically stable structures of orthocarbonates with the Ca_2CO_4 or Mg_2CO_4 stoichiometry have not been revealed in these calculations.

Assuming the stochastic nature of the used methods of crystal structure prediction and possibility that some favorable structures can be missed in the calculation, we have performed a thorough search using both evolutionary algorithms (USPEX) and *ab initio* random methods (AIRSS) within the stoichiometry of orthocarbonate M_2CO_4, where M is alkaline-earth metal, Mg, Ca, Sr, or Ba. As the result of this investigation, the structure Ca_2CO_4-*Pnma* was obtained [14]. This structure lies above the energetic convex hull in the CaO – CO_2 system, i.e. it is stable relative to the decomposition on the known phases of this system, in particular to the mixture of CaO+$CaCO_3$. Further theoretical search has also shown that the similar structures of Sr and Ba orthocarbonates, Sr_2CO_4-*Pnma* and Ba_2CO_4-*Pnma*, are also stable [15]. Recent experimental synthesis combined with single-crystal X-ray structure solution have confirmed the stability of the predicted Ca_2CO_4-*Pnma* and Sr_2CO_4-*Pnma* structures [16].

Undoubtedly, the most interesting orthocarbonate for the Earth sciences is the orthocarbonate of Mg. This compound can be readily formed within the slab subducted in the Earth's lower mantle from the locally abundant $MgCO_3$ and MgO by the simple reaction $MgCO_3 + MgO = Mg_2CO_4$. In the present study, using crystal structure prediction techniques, we performed the search of the structures in the composition Mg_2CO_4 and revealed the structure, having the chances to be formed at the Earth's lower mantle P–T conditions.

Methods

To increase the chances for finding the energetically favorable structures we have used both USPEX and AIRSS methods, each of which has apparent advantages [17]. *Ab initio* structure prediction was complemented by the prediction technique based on the known structures of silicates and sulfates with isolated

[SiO_4] and [SO_4] tetrahedrons. Mg_2CO_4 structures were produced from these structures by the corresponding replacement of the cations and consequent local optimizations. The following crystal structures have been used (numbers in parentheses indicate the number of formula units (f.u.) in the unit cell): Zn_2SiO_4-$Fd\bar{3}m$ (8), Zn_2SiO_4-$Imma$ (8), Zn_2SiO_4-$Pbca$ (8), Zn_2SiO_4-$Pnma$ (4), Zn_2SiO_4-$I\bar{4}2d$ (4) [18], Mg_2SiO_4-$Pnma$ (4) [19], Na_2SO_4-$Fddd$ (8) [20], Li_2SO_4-$P2_1/c$ (4) [21], and Ca_2CO_4-$Pnma$ (4) [14].

The calculations with the USPEX method [22–25] have been performed for 1-4 f.u. of Mg_2CO_4 at 25, 50, and 100 GPa. The seeding technique, implemented in version 10.2 of the USPEX, has been employed in all calculations. The aforementioned structures of silicates, sulfates, and orthocarbonate have been used as the seeds. Totally, around 3000 structures have been calculated at each pressure. Crystal structure prediction with AIRSS 0.9.1 [26, 27] has been performed only at 50 GPa for 2, 3, and 4 f.u. and a total of nearly 4000 structures have been generated in this calculation.

The energetic optimizations of the predicted structures have been performed within density functional theory (DFT), implemented in the VASP package [28, 29].

To take into account the temperature effect and calculate P–T phase diagram, we used the lattice dynamics method within the quasi-harmonic approximation (QHA). For this task, the lattice vibration frequencies were calculated with the PHONOPY code [30]. By our experience with P–T phase diagrams of carbonates, this technique reliably reproduces phase boundaries in the wide temperature range [2, 14, 31], up to 80-90 % of the melting temperature, if the process of dynamical disordering does not take place.

Melting temperatures of the predicted structures have been determined, using the so-called *Z-method*, based on the molecular dynamic (MD) simulations [32].

To determine the wave velocities V_p and V_s and assess anisotropy of Mg-orthocarbonates, static elastic stiffness tensor (C_{ij}) was calculated from the stress (σ)- strain (ϵ) relation $\sigma_i = C_{ij}\epsilon_j$. Based on these C_{ij} data, we calculated averages of bulk (B) and shear (G) moduli using the Voigt-Ruess-Hill scheme [33,34]. Then we have determined compression (A_B), shear (A_G), and universal anisotropy (A^U) indexes.

The details of DFT, crystal structure predictions, thermodynamic and elastic property calculations, and MD simulations are given in *Supporting information*.

FindSym program [35] and instruments of Phonopy package have been used for the symmetry determination. VESTA and ToposPro [36, 37] programs have been used for the visualization of the crystal structures and figures preparation. The topology of the structures was analysed with ToposPro and Robocrystallographer programs [37, 38].

1 Results and discussion

In the crystal structure prediction calculations at 25 and 50 GPa, USPEX has revealed the Mg_2CO_4-*Pnma* structure as the most energetically favorable. This structure has lower enthalpy than Mg_2CO_4-*Cm*, predicted by AIRSS, and structures, obtained based on the crystal structures of silicates and sulfates (Figure 1 and S1). Revealed Mg_2CO_4-*Pnma* is isostructural to Mg_2SiO_4 (forsterite) and it is not isostructural to Ca_2CO_4-*Pnma*. In the crystal structure of Ca_2CO_4-*Pnma*, Ca is coordinated by 9 or 11 oxygen atoms, while in Mg_2CO_4-*Pnma* all the Mg are 6-coordinated, with the octahedral coordination polyhedron (Figure 2a).

At 100 GPa, USPEX has found another favorable structure with monoclinic symmetry, Mg_2CO_4-$P2_1/c$. The transition from Mg_2CO_4-*Pnma* to Mg_2CO_4-$P2_1/c$ occurs at 52 GPa, and at higher pressures Mg_2CO_4-$P2_1/c$ is the most energetically favorable among considered structures (Figure 1 and S1).

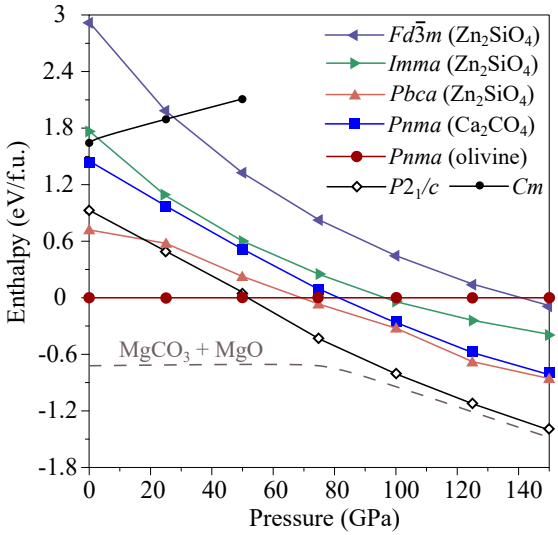

Figure 1: Enthalpy-pressure dependencies of Mg_2CO_4 structures. Isostructural compounds are indicated in brackets.

Mg_2CO_4-$P2_1/c$ is isostructural to β-Ca_2SiO_4 (larnite) and can be considered as the monoclinic analogue of Ca_2CO_4-*Pnma*. In crystal structure of Mg_2CO_4-$P2_1/c$, there are two non-equivalent Mg sites. In the first site, Mg(1) is bonded to eight oxygen atoms, forming relatively regular square antiprism, while in the second site Mg(2) is bonded to six oxygen atoms, arranged in highly deformed trigonal prism (Figure 2b). Thus, transition from Mg_2CO_4-*Pnma* to Mg_2CO_4-$P2_1/c$ is accompanied by the increase of coordination number from six to eight and six. At the transition, the volume decreases on 5.7 % (Figure S2).

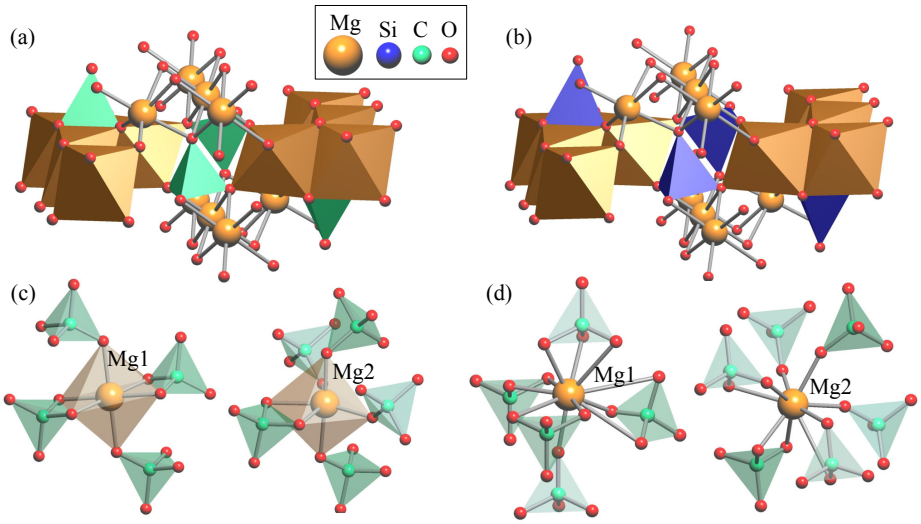

Figure 2: Comparison of crystal structures of Mg_2CO_4-*Pnma* (a) and Mg_2SiO_4-*Pnma* (b), coordination environment around Mg1 and Mg2 atoms in crystals structures Mg_2CO_4-*Pnma* (c) and Mg_2CO_4-$P2_1/c$ (d).

Structural data for the Mg_2CO_4-*Pnma* and Mg_2CO_4-$P2_1/c$ are given in the Table 1. Both structures are dynamically stable in the investigated pressure range 25-140 GPa, and there are no imaginary frequencies in their phonon dispersion curves (Figure 3, S3). In the *Supporting information*, we have also shown phonon dispersion curves of $MgCO_3$ and MgO (Figure S4) used for the construction of P–T phase diagram.

As Mg_2CO_4-*Pnma* is isostructural to γ-Ca_2SiO_4 (olivine-type) and Mg_2CO_4-$P2_1/c$ — to β-Ca_2SiO_4, the transition Mg_2CO_4-*Pnma* $\rightarrow$ Mg_2CO_4-$P2_1/c$ is the analogue of the transition γ-Ca_2SiO_4 $\rightarrow$ β-Ca_2SiO_4, realized on compression [39]. For Ca_2SiO_4, it was experimentally shown, that on heating β-Ca_2SiO_4 is transformed into another phase denoted as α'_H (Figure S5). This α'_H phase is isostructural to Ca_2CO_4-*Pnma*. Based on this similarity, the analogue of the transition β-Ca_2SiO_4 $\rightarrow$ α'_H-Ca_2SiO_4 can be suggested for Mg_2CO_4. In this case, Mg_2CO_4-$P2_1/c$ will be transformed in the new hypothetical phase Mg_2CO_4-*Pnma*-II on heating. The performed calculations of phonon dispersion curves of Mg_2CO_4-*Pnma*-II have shown the dynamical instability of this phase (Figure S6). However, the stabilization of the structure by the factors, which are not considered within QHA can not be excluded.

The performed enthalpy calculations of the Mg_2CO_4, MgO, and $MgCO_3$ structures have shown, that both Mg_2CO_4-*Pnma* and Mg_2CO_4-$P2_1/c$ lie above the energetic convex hull, i.e. they are unstable and decompose to the mixture (MgO+$MgCO_3$) at 0 K (Figure S7).

However, performed calculations of the Gibbs free energies in the temperature range of 0–3000 K have shown that above some temperature Mg_2CO_4

Table 1: Structural data of Mg_2CO_4 phases at 0 K.

P (GPa)	Space group	Lattice parameters (Å, deg)			Atom	Coordinates		
						x	y	z
50	$Pnma$ (#62)	$a = 8.926$	$b = 5.565$	$c = 4.221$	Mg1	0.000	0.000	0.500
		$\alpha = 90.0$	$\beta = 90.0$	$\gamma = 90.0$	Mg2	0.721	0.250	0.531
					C1	-0.097	0.250	0.087
					O1	-0.091	0.250	0.770
					O2	0.548	0.250	0.284
					O3	0.169	0.552	0.786
100	$P2_1/c$ (#14)	$a = 4.408$	$b = 5.383$	$c = 8.345$	Mg1	-0.022	0.000	0.693
		$\alpha = 90.0$	$\beta = 117.65$	$\gamma = 90.0$	Mg2	0.702	0.360	0.425
					C1	0.355	0.282	0.082
					O1	0.146	0.334	0.638
					O2	0.681	0.245	0.197
					O3	0.272	0.168	-0.080
					O4	0.295	0.520	0.064

became more energetically favorable than the (MgO+$MgCO_3$) mixture (Figure S8). At 20 GPa, this temperature is 2420 K, which is nearly equal to the melting temperature of $MgCO_3$-$R\bar{3}c$ (magnesite) [40] (Figure 4). The pressure decreases the temperature of transition, and at 140 GPa Mg_2CO_4-$P2_1/c$ can be synthesized from (MgO+$MgCO_3$) at temperatures higher than 1085 K. Thus, in the pressure range of 50–140 GPa, Mg_2CO_4 is formed at temperatures 250–1100 K higher than the corresponding temperatures of $MgCO_3$ melting (Figure 4). It suggests the possibility for the formation of Mg-orthocarbonate in most part of the Earth's lower mantle, at pressures higher than 50 GPa.

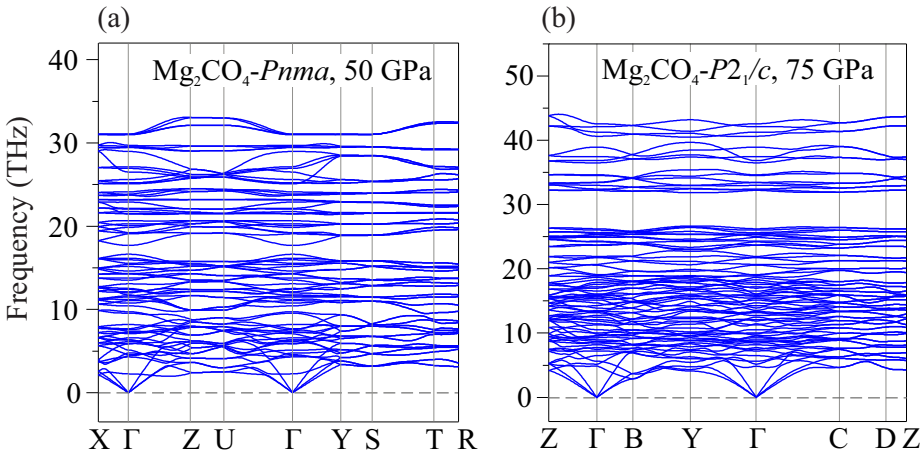

Figure 3: Phonon dispersion curves of Mg_2CO_4-*Pnma* at 50 GPa (a) and Mg_2CO_4-$P2_1/c$ at 75 GPa (b).

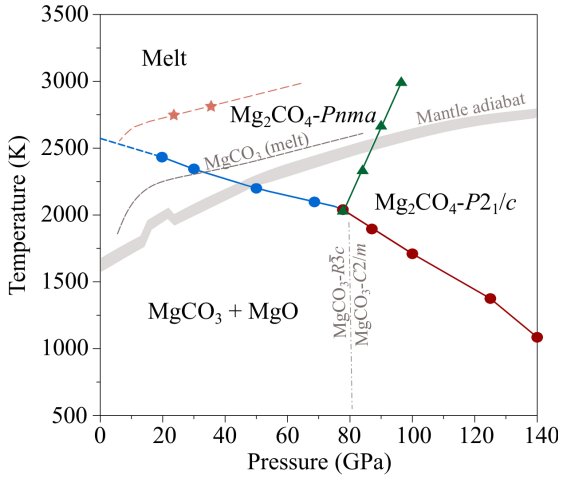

Figure 4: P–T phase diagram of Mg_2CO_4. The asterisks represent calculated melting temperatures; the grey dash-dotted line — calculated phase transition boundary of $MgCO_3$. The grey dashed line represent melting curve of $MgCO_3$ as reported by Solopova et al. [40]. Mantle adiabat is shown as grey solid line [41].

To assess the effect of Mg-orthocarbonate formation on the melting of $MgCO_3$, we have estimated melting temperatures of Mg-orthocarbonate. The obtained values of the Mg_2CO_4-*Pnma* melting temperatures at 23.7 GPa and at 35.5 GPa are 2742 K and 2819 K, respectively (Figure S9). These values are 16-18 % higher than the experimentally measured melting temperatures of magnesite and comparable with solidi of silicate rocks under lower mantle P-T

conditions [42]. The melting curve of Mg_2CO_4-*Pnma* is nearly parallel to the melting curve of magnesite, with the difference in temperature being around 500 K.

To assess the effect of orthocarbonate formation on the seismic properties of carbonate, we have also calculated the elastic stiffness tensor and compressional/shear sound velocities (V_p/V_s) for Mg-carbonate and Mg-orthocarbonate. We have not aimed the investigation of trends for the changes of elastic properties on compression or their description during $Pnma \rightarrow P2_1/c$ transition, but only the rough comparison of carbonate and orthocarbonate properties. By this reason, calculations have been performed only at 50 GPa for Mg_2CO_4-*Pnma* and magnesite structures at 0 K.

The obtained elastic properties of Mg_2CO_4 and $MgCO_3$ are summarized in Table S1 and Table S2. Obtained values of C_{ij}, B, G, V_p, and V_s for magnesite are in good agreement with the previous results of theoretical calculations [43]. According to our results, the density and both bulk and shear moduli of Mg_2CO_4-*Pnma* are higher than that of magnesite by 4-5 %. Orthocarbonate is similar to carbonate in sense of seismic velocities V_p and V_s, but orthocarbonate is more anisotropic, owning higher universal anisotropy (A^U). The value of A^U for Mg_2CO_4-*Pnma* is 0.4772, while that for magnesite is 0.2838.

Acknowledgments

This study was funded by the RFBR under research projects #20-03-00774 and #20-35-90043. Crystal structure prediction and calculation of P–T phase diagram were performed within the project #20-03-00774, while calculations of melting curve — within the project #20-35-90043. Calculations of elastic properties were supported by a state-assigned project of the IGM SB RAS.

The computations were performed using resources provided by the Novosibirsk State University Supercomputer Center.

References

[1] Gavryushkin, P. N.; Behtenova, A.; Popov, Z. I.; Bakakin, V. V.; Likhacheva, A. Y.; Litasov, K. D.; Gavryushkin, A. Toward analysis of structural changes common for alkaline carbonates and binary compounds: prediction of high-pressure structures of Li_2CO_3, Na_2CO_3, and K_2CO_3. *Crystal Growth & Design 16*, **2016**, 5612–5617.

[2] Gavryushkin, P. N.; Bekhtenova, A.; Lobanov, S. S.; Shatskiy, A.; Likhacheva, A. Y.; Sagatova, D.; Sagatov, N.; Rashchenko, S. V.; Litasov, K. D.; Sharygin, I. S.; et al. High-pressure phase diagrams of Na_2CO_3 and K_2CO_3. *Minerals 9*, **2019**, 599.

[3] Grzechnik, A.; Bouvier, P.; Farina, L. High-pressure structure of Li_2CO_3. *Journal of Solid State Chemistry 173*, **2003**, 13–19.

[4] Oganov, A. R.; Glass, C. W.; Ono, S. High-pressure phases of $CaCO_3$: Crystal structure prediction and experiment. *Earth and Planetary Science Letters 241*, **2006**, 95 – 103.

[5] Pickard, C. J.; Needs, R. J. Structures and stability of calcium and magnesium carbonates at mantle pressures. *Physical Review B 91*, **2015**, 104101.

[6] Gavryushkin, P. N.; Martirosyan, N. S.; Inerbaev, T. M.; Popov, Z. I.; Rashchenko, S. V.; Likhacheva, A. Y.; Lobanov, S. S.; Goncharov, A. F.; Prakapenka, V. B.; Litasov, K. D. Aragonite-II and $CaCO_3$-VII: New high-pressure, high-temperature polymorphs of $CaCO_3$. *Crystal Growth & Design 17*, **2017**, 6291–6296.

[7] Smith, D.; Lawler, K. V.; Martinez-Canales, M.; Daykin, A. W.; Fussell, Z.; Smith, G. A.; Childs, C.; Smith, J. S.; Pickard, C. J.; Salamat, A. Postaragonite phases of $CaCO_3$ at lower mantle pressures. *Physical Review Materials 2*, **2018**, 013605.

[8] Solomatova, N. V.; Asimow, P. D. First-principles calculations of high-pressure iron-bearing monoclinic dolomite and single-cation carbonates with internally consistent hubbard u. *Physics and Chemistry of Minerals* **2017**, 1–10.

[9] Binck, J.; Chariton, S.; Stekiel, M.; Bayarjargal, L.; Morgenroth, W.; Milman, V.; Dubrovinsky, L.; Winkler, B. High-pressure, high-temperature phase stability of iron-poor dolomite and the structures of dolomite-IIIc and dolomite-V. *Physics of the Earth and Planetary Interiors 299*, **2020**, 106403.

[10] Merlini, M.; Cerantola, V.; Gatta, G. D.; Gemmi, M.; Hanfland, M.; Kupenko, I.; Lotti, P.; Müller, H.; Zhang, L. Dolomite-IV: Candidate structure for a carbonate in the earth's lower mantle. *American Mineralogist 102*, **2017**, 1763–1766.

[11] Al-Shemali, M.; Boldyrev, A. I. Search for ionic orthocarbonates: Ab initio study of Na_4CO_4. *The Journal of Physical Chemistry A 106*, **2002**, 8951–8954.

[12] Čančarević, Ž. P.; Schoen, J. C.; Jansen, M. Possible existence of alkali metal orthocarbonates at high pressure. *Chemistry–A European Journal 13*, **2007**, 7330–7348.

[13] Yao, X.; Xie, C.; Dong, X.; Oganov, A. R.; Zeng, Q. Novel high-pressure calcium carbonates. *Physical Review B 98*, **2018**, 014108.

[14] Sagatova, D.; Shatskiy, A.; Sagatov, N.; Gavryushkin, P. N.; Litasov, K. D. Calcium orthocarbonate, Ca_2CO_4-*Pnma*: A potential host for subducting carbon in the transition zone and lower mantle. *Lithos 370-371*, **2020**, 105637.

[15] Gavryushkin, P. N.; Sagatova, D.; Sagatov, N.; Banaev, M. V. Silicate-like crystallchemistry for carbonates at high pressure. Reality or not? *IV Conference and School for Young Scientists Non-Ambient Diffraction and Nanomaterials (Book of abstracts, 19-21.10.2020)* **2020**, 38.

[16] Laniel, D.; Binck, J.; Winkler, B.; Vogel, S.; Fedotenko, T.; Chariton, S.; Prakapenka, V.; Milman, V.; Schnick, W.; Dubrovinsky, L.; Dubrovinskaia, N. Synthesis, crystal structure and structure–property relations of strontium orthocarbonate, Sr_2CO_4. *Acta Crystallographica Section B 77*, **2021**, 131–137.

[17] Oganov, A. R.; Pickard, C. J.; Zhu, Q.; Needs, R. J. Structure prediction drives materials discovery. *Nature Reviews Materials 4*, **2019**, 331–348.

[18] Kanzaki, M. High-pressure phase relations in Zn_2SiO_4 system: A first-principles study. *arXiv preprint arXiv:1903.05339* **2019**.

[19] Smyth, J. R.; Hazen, R. M. The crystal structures of forsterite and hortonolite at several temperatures up to 900 C. *American Mineralogist 58*, **1973**, 588–593.

[20] Hawthorne, F. C.; Ferguson, R. B. Anhydrous sulphates; I, Refinement of the crystal structure of celestite with an appendix on the structure of thenardite. *The Canadian Mineralogist 13*, **1975**, 181–187.

[21] Alcock, N. W.; Evans, D. A.; Jenkins, H. D. B. Lithium sulphate – a redetermination. *Acta Crystallographica Section B 29*, **1973**, 360–361.

[22] Oganov, A. R.; Glass, C. W. Crystal structure prediction using ab initio evolutionary techniques: Principles and applications. *The Journal of Chemical Physics 124*, **2006**, 244704.

[23] Oganov, A. R.; Lyakhov, A. O.; Valle, M. How evolutionary crystal structure prediction works—and why. *Accounts of Chemical Research 44*, **2011**, 227–237. PMID: 21361336.

[24] Lyakhov, A. O.; Oganov, A. R.; Stokes, H. T.; Zhu, Q. New developments in evolutionary structure prediction algorithm uspex. *Computer Physics Communications 184*, **2013**, 1172 – 1182.

[25] Bushlanov, P. V.; Blatov, V. A.; Oganov, A. R. Topology-based crystal structure generator. *Computer Physics Communications 236*, **2019**, 1 – 7.

[26] Pickard, C. J.; Needs, R. J. High-pressure phases of silane. *Physical Review Letters 97*, **2006**, 045504.

[27] Pickard, C. J.; Needs, R. J. Ab initio random structure searching. *Journal of Physics: Condensed Matter 23*, **2011**, 053201.

[28] Kresse, G.; Furthmüller, J. Efficient iterative schemes for ab initio total-energy calculations using a plane-wave basis set. *Phyical Review B 54*, **1996**, 11169–11186.

[29] Kresse, G.; Furthmüller, J. Efficiency of ab-initio total energy calculations for metals and semiconductors using a plane-wave basis set. *Computational Materials Science 6*, **1996**, 15 – 50.

[30] Togo, A.; Tanaka, I. First principles phonon calculations in materials science. *Scripta Materialia 108*, **2015**, 1–5.

[31] Gavryushkin, P. N.; Sagatov, N.; Belonoshko, A. B.; Banaev, M. V.; Litasov, K. D. Disordered aragonite: The new high-pressure, high-temperature phase of $CaCO_3$. *The Journal of Physical Chemistry C 124*, **2020**, 26467–26473.

[32] Belonoshko, A. B.; Skorodumova, N. V.; Rosengren, A.; Johansson, B. Melting and critical superheating. *Physical Review B 73*, **2006**, 012201.

[33] Hill, R. The elastic behaviour of a crystalline aggregate. *Proceedings of the Physical Society. Section A 65*, **1952**, 349–354.

[34] Hill, R. Elastic properties of reinforced solids: Some theoretical principles. *Journal of the Mechanics and Physics of Solids 11*, **1963**, 357 – 372.

[35] Stokes, H. T.; Hatch, D. M. FINDSYM: program for identifying the space-group symmetry of a crystal. *Journal of Applied Crystallography 38*, **2005**, 237–238.

[36] Momma, K.; Izumi, F. VESTA 3 for three-dimensional visualization of crystal, volumetric and morphology data. *J. Appl. Crystallogr. 44*, **2011**, 1272–1276.

[37] Blatov, V. A.; Shevchenko, A. P.; Proserpio, D. M. Applied topological analysis of crystal structures with the program package ToposPro. *Crystal Growth & Design 14*, **2014**, 3576–3586.

[38] Ganose, A. M.; Jain, A. Robocrystallographer: automated crystal structure text descriptions and analysis. *MRS Communications 9*, **2019**, 874–881.

[39] Belmonte, D.; Ottonello, G.; Zuccolini, M. V. Ab initio-assisted assessment of the CaO-SiO_2 system under pressure. *Calphad 59*, **2017**, 12 – 30.

[40] Solopova, N. A.; Dubrovinsky, L.; Spivak, A. V.; Litvin, Y. A.; Dubrovinskaia, N. Melting and decomposition of $MgCO_3$ at pressures up to 84 GPa. *Physics and Chemistry of Minerals 42*, **2015**, 73–81.

[41] Katsura, T.; Yoneda, A.; Yamazaki, D.; Yoshino, T.; Ito, E. Adiabatic temperature profile in the mantle. *Physics of the Earth and Planetary Interiors 183*, **2010**, 212 – 218. Special Issue on Deep Slab and Mantle Dynamics.

[42] Litasov, K. D.; Shatskiy, A. Carbon-bearing magmas in the earth's deep interior. In *Magmas Under Pressure*. Elsevier, **2018**, pages 43–82.

[43] Li, Z.; Stackhouse, S. Iron-rich carbonates stabilized by magnetic entropy at lower mantle conditions. *Earth and Planetary Science Letters 531*, **2020**, 115959.